frontiers in Materials

ORIGINAL RESEARCH
published: 16 April 2021
doi: 10.3389/fmats.2021.643510

# Bond Behavior of Steel-Recycled Aggregate Concrete Interface After High Temperatures and Spraying Water Cooling

*Chunheng Zhou[1], Jiazhang Cao[1] and Zongping Chen[2,3]**

*[1] School of Civil and Environmental Engineering, Ningbo University, Ningbo, China, [2] College of Civil Engineering and Architecture, Guangxi University, Nanning, China, [3] Guangxi Key Laboratory of Disaster Prevention and Engineering Safety, Guangxi University, Nanning, China*

OPEN ACCESS

**Edited by:**
*Mingxiang Xiong, Guangzhou University, China*

**Reviewed by:**
*Shan Li, National University of Singapore, Singapore*
*Yunchao Tang, Zhongkai University of Agriculture and Engineering, China*
*Mi Yu, Wuhan University, China*

***Correspondence:**
*Zongping Chen*
*zpchen@gxu.edu.cn*

**Specialty section:**
*This article was submitted to Structural Materials, a section of the journal Frontiers in Materials*

**Received:** *18 December 2020*
**Accepted:** *23 February 2021*
**Published:** *16 April 2021*

**Citation:**
*Zhou C, Cao J and Chen Z (2021) Bond Behavior of Steel-Recycled Aggregate Concrete Interface After High Temperatures and Spraying Water Cooling. Front. Mater. 8:643510. doi: 10.3389/fmats.2021.643510*

Using recycled aggregate concrete (RAC) in steel-reinforced concrete structure is an effective way to eliminate the adverse effects of recycled aggregate, which has an excellent application prospect. Fire has a great destructiveness to steel-reinforced recycled aggregate concrete (SRRAC) structure; hence, the bond performance of SRRAC after high temperature, as the prerequisite for the composite between steel and RAC, is the key problem for structural safety and the corresponding safety assessment after fire. In this article, the residual bond behaviors of steel-recycled aggregate concrete interface after different high temperatures and spraying water cooling were studied through the push-out test. The failure modes and load–slip curves were examined. The ultimate bond strength, residual bond strength, and elastic bond shear stiffness of specimens after high temperature and cooling for the regime of spraying water were evaluated and compared to that of natural air. A parametric analysis of temperature, replacement percentage, and studs was conducted. A calculation approach for the ultimate bond strength and residual bond strength of SRRAC after high temperature was developed based on the sensitive analysis of gray system theory and regression analysis. Results showed that the bond properties of SRRAC specimens after high temperature were decreased as exposure temperature increased. The cooling regime of spraying water has a more significant influence on the ultimate strength and residual strength than that of natural air. The specimens with studs on both flange and web have the highest bond properties after high temperature. In all the factors, the number of studs showed the largest gray relational degree to the bond strength of SRRAC. The developed approach provided a reliable prediction of bond strength for SRRAC after high temperature.

**Keywords: steel reinforced recycled concrete, interfacial bond-slip, high temperature, bond strength, push-out test, gray system theory**

## INTRODUCTION

Construction and demolition waste is one of the major city solid wastes, the treatment of which has become a big issue on environmental protection all over the world. In the construction and demolition wastes, concrete wastes account for a sizeable portion. Recycling use of the concrete demolition waste as recycled aggregate to partially or fully substitute natural aggregate for recycled aggregate concrete (RAC) has been recognized as an effective way to address the construction and demolition waste and related environmental problem and also offset the shortage of natural aggregate in building industry (Xiao and Li, 2012; Huda and Alam, 2014; Tang et al., 2020a).

In recent years, a large number of researches were conducted to study the mechanical properties of RAC, such as strength, elastic modulus, toughness, and stress–strain relationship (Belén and Fernando, 2011; Zhou and Chen, 2017; Xiao and Zhang, 2018). The disadvantage and discreteness of their properties due to the porous of adhered old mortar and microcrack of recycled aggregate, compared to the natural aggregate concrete, have been confirmed (Etxeberria and Vázquez, 2007; Silva and Brito, 2014). It is a key problem that has hampered the application of RAC. Therefore, RAC was considered to be used in steel reinforced concrete structures to eliminate the adverse effects of recycled aggregate by the composite between steel and concrete in many studies (Fathifazl and Razaqpur, 2009; Ma and Xue, 2015; Ma and Dong, 2019). Ma and Xue (2015) and Ma and Dong (2019) performed some cyclic loading tests on steel-reinforced recycled aggregate concrete (SRRAC) columns and joints. Fathifazl and Razaqpur (2009) conducted a study on the flexural performance of steel-reinforced recycled concrete beams. A test investigation of SRRAC frame was carried out by Xue and Zhang (2020). All the study results indicated that the encased steel in SRRAC elements can significantly reduce the negative effect of RAC on the structural performance, and SRRAC elements exhibited excellent ductility and load carry capacity under static and dynamic loading.

In SRRAC structure, the bond behavior between steel section and RAC is a prerequisite to ensure the composite of them and also the key problem of structural safety, which has been attracting the attention of a large number of researchers. Bai and Ma (2020), Liu and Fan (2019), and Liu and Xing (2020) carried out the experimental and numerical study of bond-slip between steel section and RAC with full replacement percentage (RP). The results demonstrated that the bond characteristic at the interface of SRRAC was affected by the factors such as the strength of RAC, the concrete cover thickness of protective layer, and ratio of stirrups, which was similar to that of steel and conventional concrete. A push-out test for H-shaped steel and recycled aggregate concrete with different recycled aggregate replacement ratios was conducted by Zheng and Chen (2016), indicating that the interface bonding of SRRAC increases with the replacement ratio increasing. Pandurangan and Dayanithy (2016) studied the bond strength of RAC after different treatment methods. The results showed that the treatment of recycled concrete aggregate by acid, thermal, and mechanical means can partly remove the inferior physical properties to improve the bond strength.

As the research of SRRAC further develops, the performance of RAC and SRRAC under and after the fire received attention (Chen and Zhou, 2015; Chen and Chen, 2019; Tang et al., 2020b). It is because building fires are one of the most frequent and serious disasters. The performance of SRRAC under and after the fire is a key structural performance. Among the fire-extinguishing methods, spraying water is the most common approach for building fires (Xiao and Xie, 2018). This cooling regime could cause additional damage to normal and recycled concrete (Xin and Wei, 2000; Ke and Yang, 2017). In a previous study (Chen et al., 2020), the residual bond behavior of SRRAC after exposure to elevated temperatures and natural cooling was investigated. The bond behavior of SRRAC after high temperature and cooling by different regimes, especially water spraying, needs further study.

Therefore, this study was aimed at investigating the bond behavior of steel and RAC after high temperature and cooling by spraying water. The push-out test was conducted through 18 SRRAC specimens. The parametric analysis and sensitivity analysis were carried out to study the influences of different factors on the bond strength and elastic bond shear stiffness of SRRAC. Finally, a calculation approach was developed to predict the ultimate bond strength and residual bond strength of SRRAC after high temperature.

## EXPERIMENTAL PROGRAM

### Specimen Design

To study the bond behavior between the steel section and RAC after high temperature, 18 SRRAC specimens with and without studs were designed and produced for push-out test after exposure to high temperature. The recycled aggregate RP, temperature, cooling regime, and position of studs were considered as parameters, as shown in **Table 1**. The length of specimens was 430 mm including the concrete of 400 mm and exposed steel section of 30 mm. The cross-section dimensions of specimens were 280 × 280 and 240 × 240 mm, respectively. A I14 steel was used as the steel section. The reinforcement was HRB400 longitudinal rebar with diameter of 12 mm and HPB 300 stirrups with diameter of 6 mm. The studs with a diameter of 13 mm and a length of 50 mm were mounted on the steel section with a spacing of 125 mm. The thickness of concrete cover for the steel section was set as 50 mm for the specimens without studs, while 70 mm for that with studs according to the Chinese code JGJ 138 (JGJ 138-2016, 2016). The thickness of the concrete cover for reinforcement was set as 20 mm. The dimension and the details of the specimens are shown in **Figure 1**.

### Materials

The water–cement ratio of recycled concrete was 0.4. The mix proportion was 185:463:561:1,191 by mass (water: cement: fine aggregate: coarse aggregate). The medium-fine river sand with the fineness modulus of 2.7, the apparent density of 2,530 kg/m$^3$, and the bulk density of 1,790 kg/m$^3$ was used as fine aggregate.

**TABLE 1 |** Design parameters of specimens.

| Specimens | RP/% | $T^1$/°C | Cooling regime | $C^4$/mm | Position of studs |
|---|---|---|---|---|---|
| SRRAC-1 | 0 | 20 | – | 50 | None |
| SRRAC-2 | 50 | 20 | – | 50 | None |
| SRRAC-3 | 100 | 20 | – | 50 | None |
| SRRAC-4 | 0 | 400 | WC[2] | 50 | None |
| SRRAC-5 | 50 | 400 | WC | 50 | None |
| SRRAC-6 | 100 | 400 | WC | 50 | None |
| SRRAC-7 | 0 | 600 | WC | 50 | None |
| SRRAC-8 | 50 | 600 | WC | 50 | None |
| SRRAC-9 | 100 | 600 | WC | 50 | None |
| SRRAC-10 | 100 | 400 | NC[3] | 50 | None |
| SRRAC-11 | 100 | 600 | NC | 50 | None |
| SRRAC-12 | 100 | 20 | – | 70 | Flange |
| SRRAC-13 | 100 | 400 | WC | 70 | Flange |
| SRRAC-14 | 100 | 600 | WC | 70 | Flange |
| SRRAC-15 | 100 | 400 | WC | 70 | Web |
| SRRAC-16 | 100 | 600 | WC | 70 | Web |
| SRRAC-17 | 100 | 400 | WC | 70 | Flange+Web |
| SRRAC-18 | 100 | 600 | WC | 70 | Flange+Web |

[1] *T is the highest exposure temperature.*
[2] *WC is the cooling regime of spraying water.*
[3] *NC is the cooling regime of natural air.*
[4] *C is the concrete cover thickness for steel section.*

The coarse aggregate was continuously graded recycled coarse aggregate (RCA) with diameters of 5–30 mm, which originated from crushed waste concrete with a strength class of C30. The apparent density and bulk density of RCA were 2,630 and 1,630 kg/m$^3$, respectively. The water absorption and crushing index were 2.7 and 14.1%, respectively. The P.O.32.5R ordinary Portland cement was also used. The standard cube specimens of concrete were cast to obtain the strength of RAC after exposure to different high temperature according to the Chinese code GB/T 50081 (GB/T 50081-2002, 2003). The results are shown in **Table 2**.

Besides, according to the Chinese code GB/T 228.1 (GB/T 228.1-2010, 2010), the yield strength and ultimate strength of steel section were measured, respectively, as summarized in **Table 3**.

## Test Setup and Instrumentation

### Heating Device

All specimens were cured with standard curing condition for 28 days and then were heated after 7 days in laboratory condition. The heating device was RX-45-9 heater, which has a dimension of 1,200 × 600 × 400 mm and a power of 45 kW. The highest heating temperature can reach 950°C. All of the specimens were four sides exposed in the heater, and the exposed parts of the steel section were insulated by asbestos to prevent direct thermal radiation. The heating rate was 0.5°C/min. After reaching the set temperature, the specimens in the heater were kept for a further 60 min in constant temperature according to the previous study (Zhou, 2013). The NC specimens were cooled in air under the ambient temperature of 25°C. The WC specimens were cooled using a water sprinkler. The duration of water spraying was 120 min. For each condition and cooling regime, the concrete cube specimens were prepared the same as the corresponding SRRAC specimens.

### Push-Out Test Device and Measuring Method

After cooling, the specimens were uniformly placed for 3 days and then tested under a servo testing machine. The push-out tests were conducted under incremental displacement controlled with a constant rate of 0.002 mm/s. When the cracks on the surface of specimens were observed obviously, or the slip reached 8 mm, the specimen was recognized to be damaged; meanwhile, the test was ended. Four linear variable differential transformers (LVDT) were installed on the setup and specimens to measure the slips. Two of the LVDTs were used to obtain the slip of the loaded end and the free end, and the other two were mounted on the top of specimens and the fixed end of setup. The setup and instrumentation are shown in **Figure 2**.

# EXPERIMENTAL RESULTS AND ANALYSIS

## The Mass Loss Rate of Specimens

The mass loss of each specimen after high temperature was obtained and shown in **Figure 3**. In the figure, $L$ is the mass loss rate; $T$ is exposure temperature. It can be seen that the mass loss rate of SRRAC specimens increases with the increase

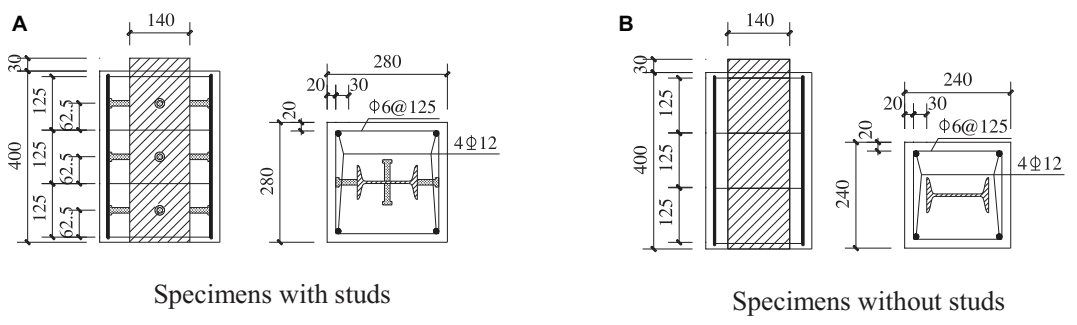


**FIGURE 1 |** Dimensions and configurations of specimens. **(A)** Specimens with studs. **(B)** Specimens without studs.

**TABLE 2 |** Compressive strength of RAC (MPa).

| Temperature | 20°C | 400°C | 600°C |
|---|---|---|---|
| Cooling regime of WC | 41.4 | 27.2 | 22.1 |
| Cooling regime of NC | 41.4 | 25.7 | 23.9 |

**TABLE 3 |** Mechanical properties of steel section.

| Temperature | 20°C | 400°C | 600°C |
|---|---|---|---|
| $f_y$[1]/MPa | 344.7 | 359.9 | 329.6 |
| $f_u$[2]/MPa | 434.4 | 452.1 | 410.3 |

[1] *$f_y$ is the yield strength.*
[2] *$f_u$ is the ultimate strength.*

of the maximum temperature due to the evaporation of water after exposure to high temperature. The cooling regime has no significant effect on the mass loss rate of specimens because there was not a lot of mass loss during the cooling process.

## Failure Modes of Specimens

The failure modes of specimens with or without studs are different. For SRRAC specimens without studs, the slip first occurred at the loaded end of specimens in the initial loading stage. When the load increased to greater than 80% of the ultimate load, the free end of specimens started to slip, and the cracks in concrete were observed near the steel flange. With the load increased continuously, the cracks developed outward and propagated to the loaded end. Subsequently, the cracks propagated the whole height of specimens at peak load state, as shown in **Figure 4A**. After peak load, no new cracks occurred. The specimens that suffered higher temperature produced more cracks in the process of failure owing to the initial damage of high temperature. The replacement of the recycled concrete had insignificant influence on the failure modes of specimens.

For SRRAC specimens with studs, the failure process was similar to that of the specimens without studs in the initial loading stage. However, when the cracks developed near the studs, some lateral and inclined cracks appeared on the concrete at this place. In the specimens with suds on both flange and web, the lateral and inclined cracks were relatively more and wider. In the specimens with studs only on flange, the cracks were relatively less and thin, as shown in **Figure 4B**. After the test and removing the concrete cover, the bending deformation of studs can be found, which indicated that the studs played an important role to resist the slip between steel and concrete, as shown in **Figure 4B**.

The failure mode of WC cooling specimens was similar to that of NC cooling specimens. Hence, the cooling regime has no influence on the failure more of the specimens.

## Load–Slip Curves

The load–slip curves (*P–S* curves) of SRRAC specimens were obtained by the loading equipment and LVDTs, as shown in **Figure 5**. It can be seen that the shapes of *P–S* curves of the loaded end of the specimens without studs were similar to that of the free end, while they were quite different for the specimens with studs. During the loading process, the slip of all the specimens occurred at the loaded end first, while the slip at the free end occurred later. The slip hysteresis phenomenon between the loaded end and the free end was more obvious in the specimens with studs. The maximum temperature had almost no effect on the hysteresis phenomenon. The slip process of all specimens could be divided into three stages, which include ascending stage, descending stage, and residual stage. However, in the specimens without studs, there was no obvious descending stage, and the load did not decrease significantly after peak load. For the specimens with studs on the flange, there was no obvious residual stage, and the specimens were failure suddenly after peak load. The ascending stage of the *P–S* curves for most specimens with studs showed an elastic-plastic stage, whereas it was almost not observed in the specimens without studs.

# PARAMETRIC ANALYSIS

## Bond Properties

According to the *P–S* curves, a series of bond properties, including the ultimate load $P_u$, the residual load $P_r$, the ultimate

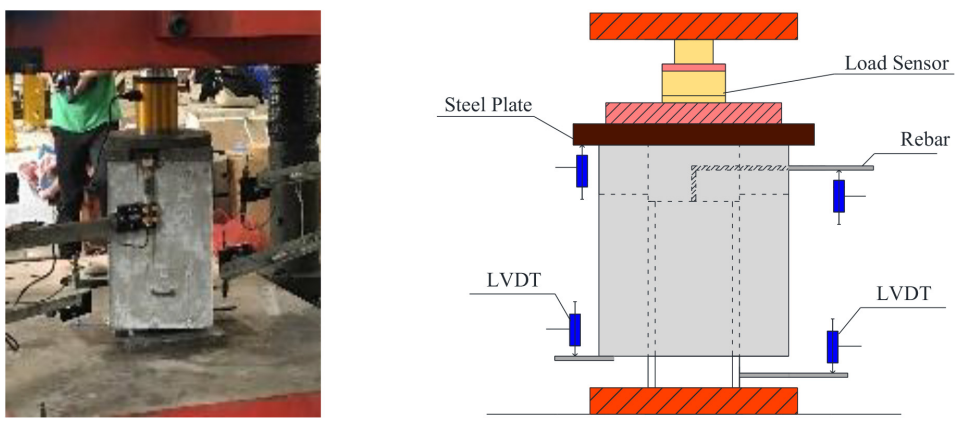


**FIGURE 2 |** Setup and instrumentation for push-out test.

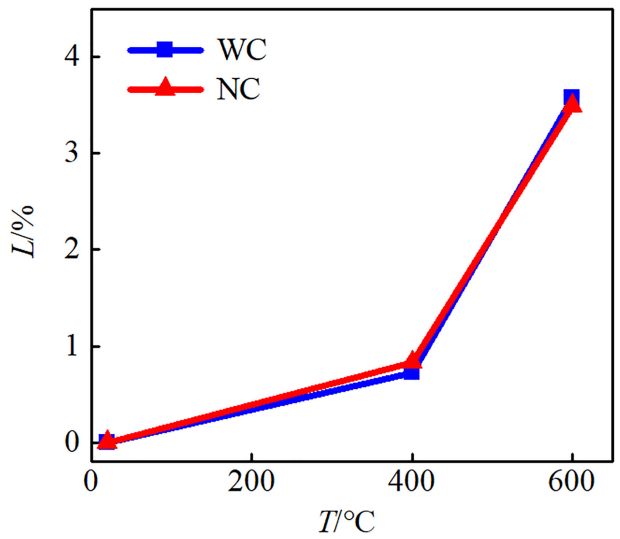


**FIGURE 3 |** The mass loss rate of specimens.

bond strength $\tau_u$, the residual bond strength $\tau_r$, and elastic bond shear stiffness $K_e$, were obtained and tabulated in **Table 4**. The ultimate bond strength was defined as the bond stress between the steel section and concrete on the peak load of *P*–*S* curves, which has been used to analyze the bond behavior by Nezamian and Al-Mahaidi (2006). The residual bond strength was taken as the residual stress without further reduction after large slip due to the friction force between steel section and concrete, which has been used to analyze the residual bond behavior by Nezamian and Al-Mahaidi (2006). The ultimate bond strength $\tau_u$ and the residual bond strength $\tau_r$ could be calculated according to Eq. (1). The elastic bond shear stiffness was defined as the secant stiffness at the point of 0.8 $P_u$ of the ascending stage of the *P*–*S* curves of the loaded end in this study.

$$\tau = \frac{P}{C_a l_a} \tag{1}$$

where $C_a$ is the perimeter of the steel section; $l_a$ is the embedment length of the steel section.

## Effect of Temperature

The effect of temperature on the bond properties of SRRAC is shown in **Figure 6**. It can be noticed that the ultimate bond strength, residual bond strength, and elastic bond shear stiffness of SRRAC decreased with the increase of temperature. The influence of temperature on the bond strength for the specimens without studs was more significant than that of the specimens with studs. In the 600°C specimens without studs, the ultimate bond strength and residual bond strength were reduced by 87.9 and 81.1%, respectively, compared to that of the specimens without heating. As for the 600°C specimens with studs, the ultimate bond strength and residual bond strength were just reduced by 12.4 and 13.4%, respectively. The results can be attributed to that the interfacial bond strength between the steel section and RAC in the specimens without studs was mainly controlled by the cohesive force and friction force, whereas the interfacial strength of the specimens with studs was dominantly by the mechanic interlock force. The high temperature has a more considerable effect on the cohesive force and friction force. For the specimens without studs, with the increase of the temperature, the degradation of ultimate bond strength was most significant in all bond properties. The ultimate bond strength of the 400°C specimens was 24.3–35.5% of that for the specimens without heating, while the value was just 12.1–22.0% for 600°C specimens.

## Effect of Cooling Regime

The influence of cooling regime on the bond behavior of SRRAC is shown in **Figure 7**. It can be seen that after 400°C, the bond properties of the specimens for WC cooling regime were lower than that of NC cooling regime. Compared to the NC cooling specimens, the ultimate bond strength, residual bond strength, and shear stiffness of the WC cooling specimens were further reduced by 13.2, 9.8, and 28.4%, respectively. The results indicated that the cooling regime of WC made the interfacial performance further deteriorate for the specimens after high temperature. It was because, in the WC regime, the external temperature of the specimens decreased rapidly while the internal temperature remained

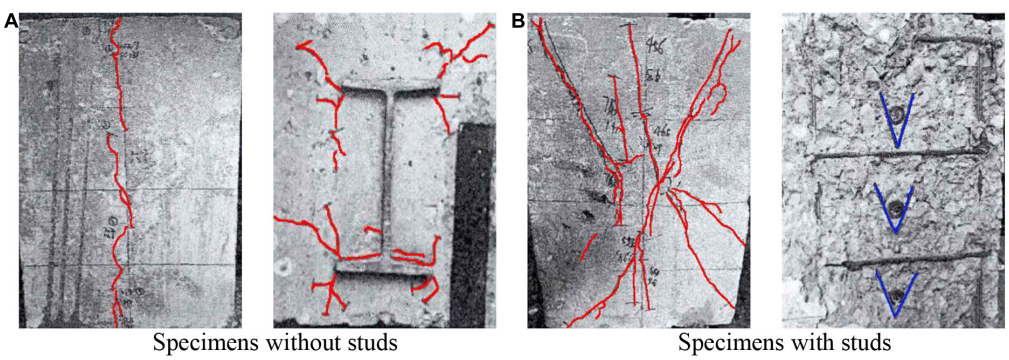


**FIGURE 4 |** Failure modes of specimens. **(A)** Specimens without studs. **(B)** Specimens with studs.

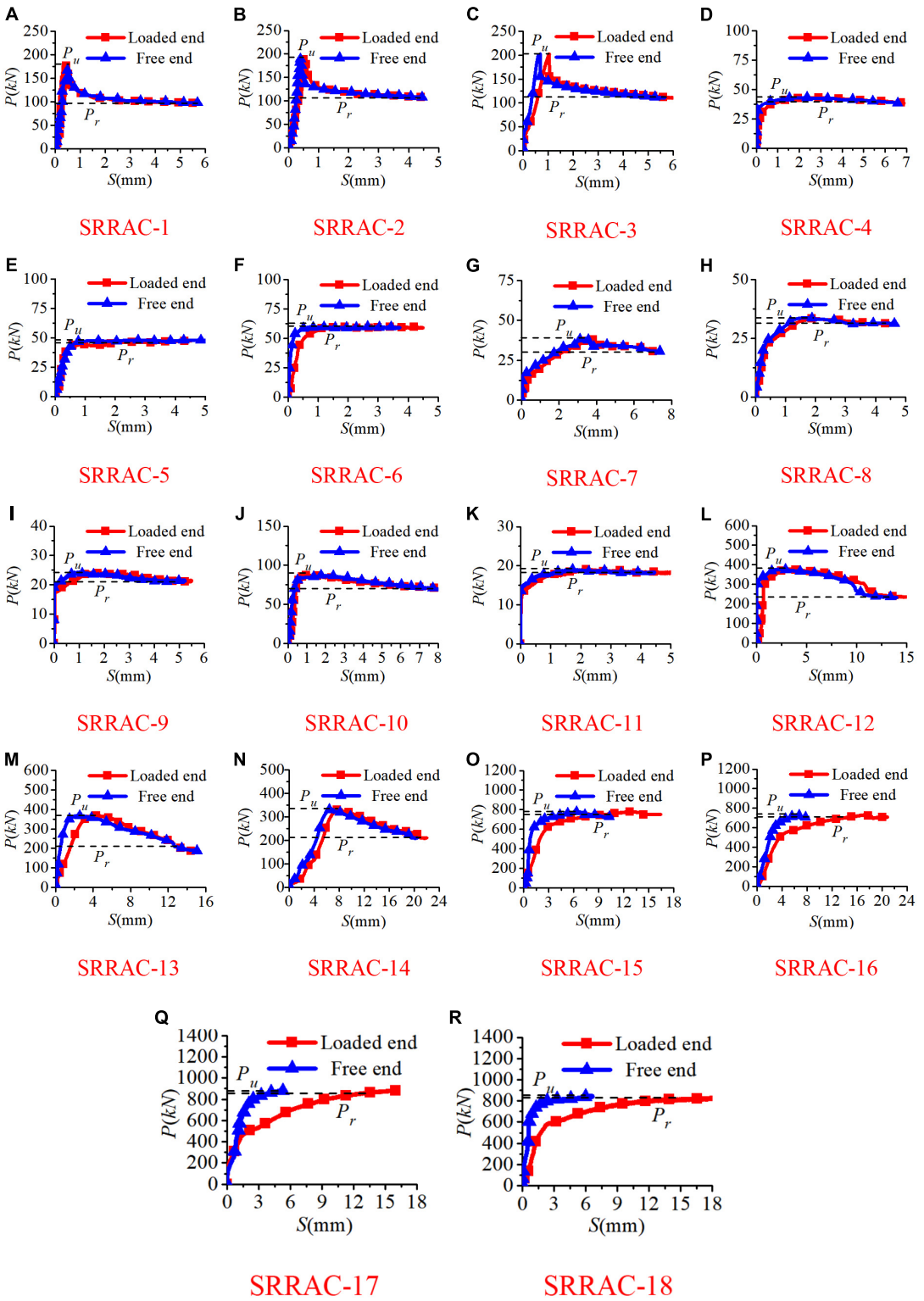


**FIGURE 5 |** *P–S* curves of specimens. **(A)** SRRAC-1. **(B)** SRRAC-2. **(C)** SRRAC-3. **(D)** SRRAC-4. **(E)** SRRAC-5. **(F)** SRRAC-6. **(G)** SRRAC-7. **(H)** SRRAC-8. **(I)** SRRAC-9. **(J)** SRRAC-10. **(K)** SRRAC-11. **(L)** SRRAC-12. **(M)** SRRAC-13. **(N)** SRRAC-14. **(O)** SRRAC-15. **(P)** SRRAC-16. **(Q)** SRRAC-17. **(R)** SRRAC-18.

**TABLE 4 |** Bond properties of SRRAC after high temperature.

| Specimens | $P_u$/kN | $P_r$/kN | $\tau_u$/MPa | $\tau_r$/MPa | $K_e$/kN·mm$^{-1}$ |
|---|---|---|---|---|---|
| SRRAC-1 | 176.2 | 97.1 | 0.80 | 0.44 | 380.9 |
| SRRAC-2 | 191.2 | 106.6 | 0.86 | 0.48 | 350.6 |
| SRRAC-3 | 202.4 | 111.9 | 0.91 | 0.51 | 199.4 |
| SRRAC-4 | 42.9 | 39.2 | 0.19 | 0.18 | 73.3 |
| SRRAC-5 | 48.4 | 47.4 | 0.22 | 0.21 | 101.9 |
| SRRAC-6 | 60.1 | 59.0 | 0.27 | 0.25 | 100.9 |
| SRRAC-7 | 38.8 | 30.2 | 0.18 | 0.14 | 13.2 |
| SRRAC-8 | 34.2 | 31.2 | 0.15 | 0.14 | 30.1 |
| SRRAC-9 | 24.4 | 21.2 | 0.11 | 0.10 | 60.5 |
| SRRAC-10 | 87.2 | 71.9 | 0.39 | 0.32 | 157.5 |
| SRRAC-11 | 19.2 | 18.6 | 0.09 | 0.08 | 43.0 |
| SRRAC-12 | 378.5 | 243.5 | 1.71 | 1.10 | 323.7 |
| SRRAC-13 | 367.5 | 207.5 | 1.66 | 0.94 | 127.4 |
| SRRAC-14 | 331.5 | 211.0 | 1.50 | 0.95 | 43.6 |
| SRRAC-15 | 778.6 | 750.5 | 3.52 | 3.39 | 213.5 |
| SRRAC-16 | 730.0 | 704.0 | 3.30 | 3.18 | 92.8 |
| SRRAC-17 | 882.0 | 871.5 | 3.98 | 3.94 | 114.2 |
| SRRAC-18 | 850.0 | 846.5 | 3.84 | 3.82 | 127.6 |

high. In this process, the temperature stress caused by the inside and outside differences in temperature, which was negligible in the NC regime, led to a larger number of cracks that the concrete was further damaged. However, there was no significant effect on the bond behavior of specimens after high temperature of 600°C between the two cooling regimes. It was because the large number of cracks caused by the expansion under the heating process makes more dominant damage than that caused by the temperature variations between the internal and external parts of concrete under the cooling process.

## Effect of RP

**Figure 8** shows the influence of RP on bond properties of SRRAC after high temperature. In the figure, the relative ultimate bond strength, relative residual bond strength, and relative elastic bond shear stiffness for specimens after high temperature compared to that without heating, namely, $\tau_u^T/\tau_u^0$, $\tau_r^T/\tau_r^0$, and $K_e^T/K_e^0$, were regarded as the bond degradation index for analysis. It can be seen clearly from the figure that, after exposure to 400°C, the relative ultimate bond strength and residual bond strength had no significant difference with the increase of RP. However, after exposure to 600°C, the relative ultimate bond strength and residual bond strength were decreased as RP increased. Compared to the specimen of RP = 0%, $\tau_u^T/\tau_u^0$ and $\tau_r^T/\tau_r^0$ for the specimen of RP = 50% reduced by 22.7 and 8.2%, respectively. The reduced values for that of RP = 100% were 46.2 and 38.4%, respectively. It indicated that the high temperature had a great influence on the bond strength between steel section and recycled concrete when RP increased. It was because the mechanical property of the new–old interfacial transition zone in recycled concrete was more liable to be affected by high temperature. On the contrary, the relative elastic bond shear stiffness was increased when RP increased.

## Effect of Studs

The influence of the stud position on the bond behavior of SRRAC after high temperature is shown in **Figure 9**. It can be seen that with or without studs and the setting position of studs had a significant influence on the ultimate bond strength and residual bond strength of the specimens. After high temperature, the ultimate bond strength and the residual bond strength of the specimens with studs were higher than those of the specimens without studs. The ultimate bond strength and residual bond strength of the specimens with studs on both the flange and the web were the highest. The ultimate bond strength and residual bond strength of the specimens with studs only on the web were higher than those with studs only on the flange. It was indicated that setting studs on the web exhibited the best bond strength of SRRAC after high temperature. After high temperature, the location of the studs had a small effect on the elastic bond shear stiffness. The elastic bond shear stiffness exhibited the largest value for the specimens with studs on the web after high temperature.

# SENSITIVITY ANALYSIS

The results of the parametric analysis presented that the bond strength of SRRAC after high temperature was influenced by a variety of factors, and all of the factors were interactive. Therefore, a sensitivity analysis was conducted using a

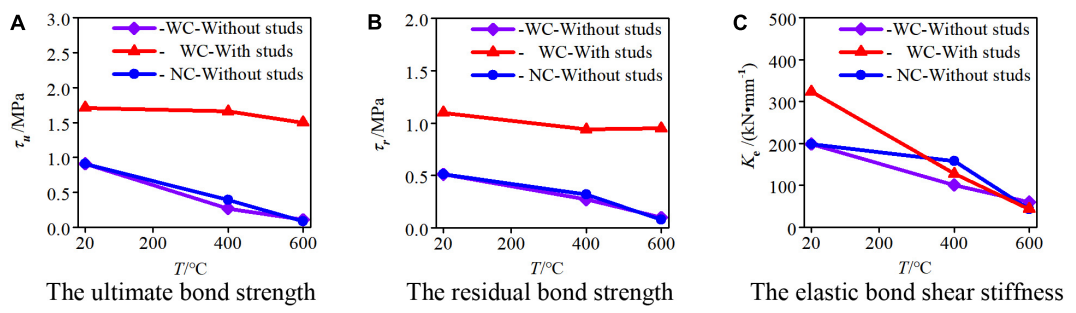


**FIGURE 6 |** Effect of temperature. **(A)** The ultimate bond strength. **(B)** The residual bond strength. **(C)** The elastic bond shear stiffness.

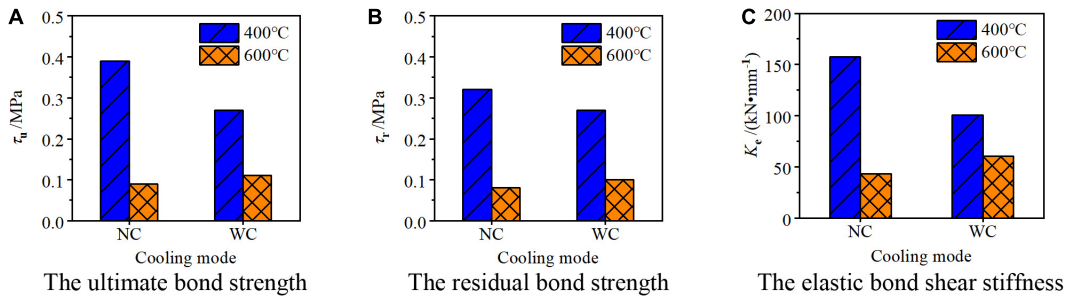


**FIGURE 7 |** Effect of cooling regime. **(A)** The ultimate bond strength. **(B)** The residual bond strength. **(C)** The elastic bond shear stiffness.

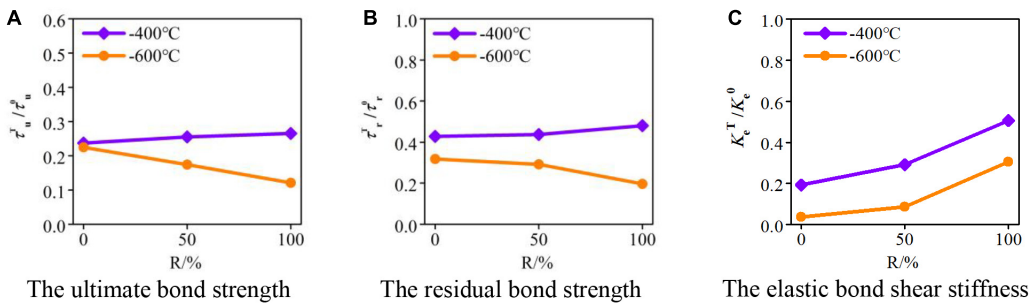


**FIGURE 8 |** Effect of RP. **(A)** The ultimate bond strength. **(B)** The residual bond strength. **(C)** The elastic bond shear stiffness.

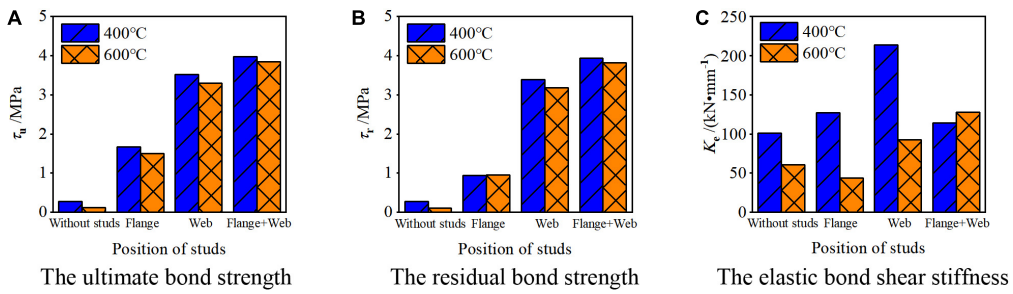


**FIGURE 9 |** Effect of studs. **(A)** The ultimate bond strength. **(B)** The residual bond strength. **(C)** The elastic bond shear stiffness.

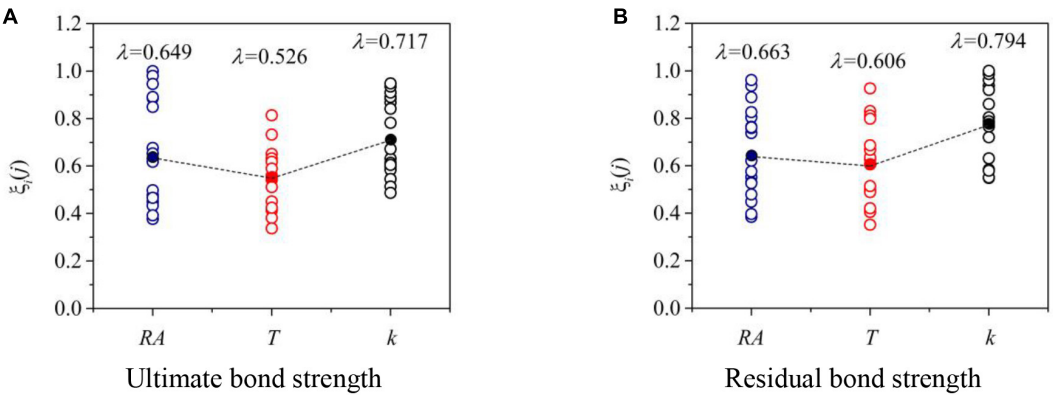


**FIGURE 10 |** Results of gray relational coefficient and degree. **(A)** Ultimate bond strength. **(B)** Residual bond strength.

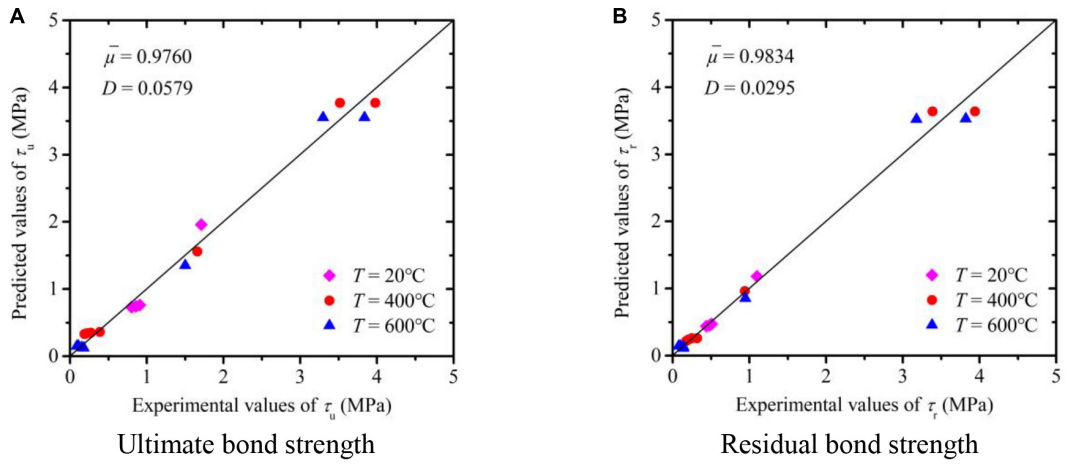


**FIGURE 11 |** Comparison of experimental and predicted $\tau_U$ and $\tau_r$. **(A)** Ultimate bond strength. **(B)** Residual bond strength.

mathematical gray system theory (GST) to examine the parametric sensitivity of the ultimate bond strength and residual bond strength. GST is a reliable method for sensitivity analysis because of its effectiveness in dealing with uncertain and complicated data. It has been successfully applied in the analysis of mechanical properties of normal and recycled concrete (Li and Cai, 2018; Xu and Zhao, 2019).

The ultimate bond strength and residual bond strength were determined as the reference matrix $X_0(j)$. The RCA replacement ratio ($RA$), temperature ($T$), and number of studs per unit length ($k$) were considered as the relative matrix $X_1(j)$, $X_2(j)$, $X_3(j)$, respectively. Based on the normalized data, the gray relational coefficient $\xi_i(j)$ can be expressed as follows:

$$\xi(\mathrm{j}) = \frac{\min\limits_{\mathrm{i}} \min\limits_{\mathrm{j}} \Delta_{\mathrm{i}}(\mathrm{j}) + \rho \max\limits_{\mathrm{i}} \max\limits_{\mathrm{j}} \Delta_{\mathrm{i}}(\mathrm{j})}{\Delta_{\mathrm{i}}(\mathrm{j}) + \rho \max\limits_{\mathrm{i}} \max\limits_{\mathrm{j}} \Delta_{\mathrm{i}}(\mathrm{j})} \tag{2}$$

$$\Delta_i(j) = \left| X_0'(j) - X_i'(j) \right| \tag{3}$$

where ρ is a coefficient and equal to 0.5 (Liu and Yang, 2017); $X_0'(j)$ is the normalization of the reference matrix, and $X_i'(j)$ is the normalization of the relative matrix and can be determined as follows:

$$X_0'(j) = \frac{X_0(j)}{\frac{1}{n}\sum_{j=1}^{n} X_0(j)} \tag{4}$$

$$X_i'(j) = \frac{X_i(j)}{\frac{1}{n}\sum_{j=1}^{n} X_i(j)} \tag{5}$$

The gray relational degree λ, which is used to measure the correlation between the reference matrix and the comparative matrix, is given as follows:

$$\lambda = \frac{1}{n}\sum_{j=1}^{n} \xi_i(j) \tag{6}$$

In GST, λ close to 1 represents the strong correlation, whereas λ close to 0 indicates a negligible correlation (Liu and Yang, 2017). The results of the gray relational coefficient $\xi_i(j)$ and the gray relational degree λ for the parameters are shown in **Figure 10**. As can be seen, all the λ were higher than 0.5, indicating a high correlation. The most sensitive parameter on both ultimate bond strength and residual bond strength is the number of studs, which had the highest gray relational degree of 0.717 and 0.794, respectively.

## CALCULATION OF ULTIMATE AND RESIDUAL BOND STRENGTH

Based on the above results of GST analysis, the calculation of ultimate bond strength and residual bond strength of SRRAC after high temperature ($T \leq 600°C$) can be conducted according to Eq. (7) and Eq. (8). In the equation, the coefficients were determined according to the regression analysis of corresponding parameters.

$$\tau_{\mathrm{u}} = 1.4702k + 0.0309R - 0.0011T - 0.0502C + 3.2608 \tag{7}$$

$$\tau_{\mathrm{r}} = 1.7741k + 0.0339R - 0.0005T - 0.0984C + 5.3694 \tag{8}$$

The comparison of experimental ultimate bond strength and residual bond strength for SRRAC after high temperature with the corresponding bond strengths calculated by Eq. (7) and Eq. (8) is shown in **Figure 11**. The average ratio of the calculated ultimate bond strength to experimental values was 0.9760 with a variance of 0.0579. The average ratio of the calculated residual bond strength to experimental values was 0.9834 with a variance of 0.0295. The predicted results showed a satisfactory agreement well with the experimental results.

## CONCLUSION

(1) When the maximum temperature was less than 600°C, the mass loss of SRRAC specimens after high temperature was all increased with the increase of the temperature. With the increase of the temperature, the bond properties of SRRAC specimens after high temperature decreased gradually. The bond properties affected by the temperature were more significant for the specimens without studs than those of the specimens with studs.

(2) The mass loss was not affected by the cooling regime. The WC cooling has a more significant influence on the ultimate strength and residual strength of the specimens after high temperature of 400°C than that of NC. The decrease of the ultimate bond strength, residual bond strength, and elastic bond shear stiffness for the WC specimens after high temperature was more significant.

(3) After a relatively low temperature of 400°C, RP has no significant influence on the bond strength. After a relatively high temperature of 600°C, the bond strength decreased as RP increased. The relative elastic bond shear stiffness was increased when RP increased.

(4) When the maximum temperature was less than 600°C, the specimens with studs on both flange and web exhibited the highest ultimate strength and residual strength after high temperature. The ultimate strength and residual strength of the specimens with studs only on web were higher than those of the specimens with studs only on flange.

(5) RP, temperature, and the number of studs had a relatively strong correlation with the bond strength of SRRAC after high temperature lower than 600°C. Among the factors, the number of studs showed the largest gray relational degree versus the bond strength of specimens, while the temperature is the lowest one.

(6) The predicted results of ultimate bond strength and residual bond strength using the proposed equations correlated well with the experimental results.

## DATA AVAILABILITY STATEMENT

The original contributions presented in the study are included in the article/supplementary material, further inquiries can be directed to the corresponding author.

## AUTHOR CONTRIBUTIONS

CZ: investigation, data curation, and writing – original draft preparation. ZC: writing – review and editing. JC: visualization. All authors contributed to the article and approved the submitted version.

## FUNDING

This work was supported by the Natural Science Foundation of Zhejiang Province (LQ20E080003), Systematic Project of Guangxi Key Laboratory of Disaster Prevention and Structural Safety (2019ZDK017), and Special fund project for "Bagui" scholars, grant number ([2019] No.79).

## REFERENCES

Bai, G. L., and Ma, J. F. (2020). Study on the interfacial bond slip constitutive relation of I-section steel and fully recycled aggregate concrete. *Constr. Build. Mater.* 238:117688. doi: 10.1016/j.conbuildmat.2019.117688

Belén, G. F., and Fernando, M. A. (2011). Stress-strain relationship in axial compression for concrete using recycled saturated coarse aggregate. *Constr. Build. Mater.* 25, 2335–2342. doi: 10.1016/j.conbuildmat.2010.11.031

Chen, Z. P., and Chen, J. J. (2019). Residual properties of recycled concrete after exposure to high temperatures. *Mag. Concrete Res.* 71, 781–793. doi: 10.1680/jmacr.17.00503

Chen, Z. P., and Zhou, C. H. (2015). Axial compression performance and bearing capacity calculation of steel reinforced recycled concrete column under high temperature. *J. Build. Eng.* 36, 70–81. doi: 10.14006/j.jzjgxb.2015.12.009 (In Chinese),

Chen, Z. P., Zhou, J., Ban, M. G., and Xinyue, W. (2020). Residual bond behavior of steel reinforced recycled aggregate concrete after exposure to elevated temperatures[J]. *Front. Mater.* 7:142. doi: 10.3389/fmats.2020.00142

Etxeberria, M., and Vázquez, E. (2007). Influence of amount of recycled coarse aggregates and production process on properties of recycled aggregate concrete. *Cem. Concr. Res.* 13, 735–742. doi: 10.1016/j.cemconres.2007.02.002

Fathifazl, G., and Razaqpur, A. G. (2009). Flexural performance of steel-reinforced recycled concrete beams. *ACI Struct. J.* 106, 858–867. doi: 10.1016/j.jhydrol.2009.08.013

GB/T 50081-2002 (2003). *Standard for Test Method of Mechanical Properties on Ordinary Concrete*. Beijing: China Ministry of Construction (In Chinese).

GB/T 228.1-2010 (2010). *Metallic Materials-Tensile Testing-Part 1; Method of Test at Room Temperature*. Beijing: China National Standardization Management Committee (In Chinese).

Huda, S. B., and Alam, M. S. (2014). Mechanical behavior of three generations of 100% repeated recycled coarse aggregate concrete. *Constr. Build. Mater.* 65, 574–582. doi: 10.1016/j.conbuildmat.2014.05.010

JGJ 138-2016. (2016). *Code for Design of Composite Structures*. Beijing: China Ministry of Construction (In Chinese).

Ke, X. J., and Yang, C. H. (2017). Influences of cooling methods on mechanical properties of recycled aggregate concrete after exposure to high temperature. *J. Build. Mater.* 20, 794–800. doi: 10.3969/j.issn.1007-9626.2017.05.023 (In Chinese),

Li, B. X., and Cai, L. H. (2018). Predicting service life of concrete structure exposed to sulfuric acid environment by grey system theory. *Int. J. Civ. Eng.* 16, 1017–1027. doi: 10.1007/s40999-017-0251-2

Liu, C., and Fan, Z. Y. (2019). Experimental study on bond behavior between section steel and RAC under full replacement ratio. *KSCE J. Civ. Eng.* 23, 1159–1170. doi: 10.1007/s12205-019-0702-1

Liu, C., and Xing, L. (2020). Numerical study of bond slip between section steel and recycled aggregate concrete with full replacement ratio. *Appl. Sci.* 10:887. doi: 10.3390/app10030887

Liu, S., and Yang, Y. (2017). *Grey Data Analysis*. Singapore: Springer Singapore, 978–981.

Ma, H., and Dong, J. (2019). Cyclic loading tests and shear strength of composite joints with steel-reinforced recycled concrete columns and steel beams. *Eng. Struct.* 199:109605. doi: 10.1016/j.engstruct.2019.109605

Ma, H., and Xue, J. Y. (2015). Cyclic loading tests and shear strength of steel reinforced recycled concrete short columns. *Eng. Struct.* 92, 55–68. doi: 10.1016/j.engstruct.2015.03.009

Nezamian, A., and Al-Mahaidi, R. (2006). Bond strength of concrete plugs embedded in tubular steel piles under cyclic loading. *Can. J. Civil. Eng.* 33, 111–125. doi: 10.1139/l05-091

Pandurangan, K., and Dayanithy, A. (2016). Influence of treatment methods on the bond strength of recycled aggregate concrete. *Constr. Build. Mater.* 120, 212–221. doi: 10.1016/j.conbuildmat.2016.05.093

Silva, R. V., and Brito, J. D. (2014). The influence of the use of recycled aggregates on the compressive strength of concrete: a review. *Eur. J. Environ. Civ. Eng.* 19, 825–849. doi: 10.1080/19648189.2014.974831

Tang, Y., Fang, S., Chen, J., Ma, L., Li, L., and Wu, X. (2020a). Axial compression behavior of recycled-aggregate-concrete-filled GFRP–steel composite tube columns. *Eng. Struct.* 216:110676. doi: 10.1016/j.engstruct.2020.110676

Tang, Y. C., Feng, W. H., Feng, W. X., Chen, J. M., Bao, D. J., and Li, L. J. (2020b). Compressive properties of rubber-modified recycled aggregate concrete subjected to elevated temperatures. *Construct. Build. Mater.* 121181. *VQ, doi: 10.1016/j.conbuildmat.2020.121181

Xiao, J. Z., and Li, W. G. (2012). Recent studies on mechanical properties of recycled aggregate concrete in China – a review. *Sci. China Technol. Sci.* 55, 1463–1480. doi: 10.1007/s11431-012-4786-9

Xiao, J. Z., and Xie, Q. H. (2018). Study on high-performance concrete at high temperatures in China (2004–2016) – an updated overview. *Fire Saf. J.* 95, 11–24. doi: 10.1016/j.firesaf.2017.10.007

Xiao, J. Z., and Zhang, K. J. (2018). Variability of stress-strain relationship for recycled aggregate concrete under uniaxial compression loading. *J. Clean. Prod.* 181, 753–771. doi: 10.1016/j.jclepro.2018.01.247

Xin, L., and Wei, S. (2000). Effect of heating and cooling regimes on residual strength and microstructure of normal strength and high-performance concrete. *Cement Concrete Res.* 30, 379–383. doi: 10.1016/S0008-8846(99)00264-1

Xu, J. J., and Zhao, X. Y. (2019). Parametric sensitivity analysis and modelling of mechanical properties of normal-and high-strength recycled aggregate concrete using grey theory, multiple nonlinear regression and artificial neural networks. *Constr. Build. Mater.* 211, 479–491. doi: 10.1016/j.conbuildmat.2019.03.234

Xue, J. Y., and Zhang, X. (2020). Pseudo-dynamic test investigation of recycled concrete-encased steel frame. *J. Build. Eng.* 32:101834. doi: 10.1016/j.jobe.2020.101834

Zheng, H. H., and Chen, Z. P. (2016). Bond behavior of H-shaped steel embedded in recycled aggregate concrete under push-out loads. *Int. J. Steel Struct.* 16, 347–360. doi: 10.1007/s13296-016-6008-y

Zhou, C. H. (2013). *Experimental Research and Theoretical Analysis on Mechanical Behaviors of Steel Reinforced Recycled Aggregate Concrete Columns after fire (High Temperature)*. Liuzhou: Guangxi University (In Chinese).

Zhou, C. H., and Chen, Z. P. (2017). Mechanical properties of recycled concrete made with different types of coarse aggregate. *Constr. Build. Mater.* 134, 497–506. doi: 10.1016/j.conbuildmat.2016.12.163

**Conflict of Interest:** The authors declare that the research was conducted in the absence of any commercial or financial relationships that could be construed as a potential conflict of interest.